ACS APPLIED MATERIALS & INTERFACES
Research Article
www.acsami.org

Thermal Conduction in Vertically Aligned Copper Nanowire Arrays and Composites

Michael T. Barako,[†] Shilpi Roy-Panzer,[‡] Timothy S. English,[†] Takashi Kodama,[†] Mehdi Asheghi,[†] Thomas W. Kenny,[†] and Kenneth E. Goodson*[,†]

[†]Department of Mechanical Engineering and [‡]Department of Electrical Engineering, Stanford University, Stanford, California 94305, United States

Supporting Information

ABSTRACT: The ability to efficiently and reliably transfer heat between sources and sinks is often a bottleneck in the thermal management of modern energy conversion technologies ranging from microelectronics to thermoelectric power generation. These interfaces contribute parasitic thermal resistances that reduce device performance and are subjected to thermomechanical stresses that degrade device lifetime. Dense arrays of vertically aligned metal nanowires (NWs) offer the unique combination of thermal conductance from the constituent metal and mechanical compliance from the high aspect ratio geometry to increase interfacial heat transfer and device reliability. In the present work, we synthesize copper NW arrays directly onto substrates via templated electrodeposition and extend this technique through the use of a sacrificial overplating layer to achieve improved uniformity. Furthermore, we infiltrate the array with an organic phase change material and demonstrate the preservation of thermal properties. We use the 3ω method to measure the axial thermal conductivity of freestanding copper NW arrays to be as high as 70 W m^{-1} K^{-1}, which is more than an order of magnitude larger than most commercial interface materials and enhanced-conductivity nanocomposites reported in the literature. These arrays are highly anisotropic, and the lateral thermal conductivity is found to be only 1−2 W m^{-1} K^{-1}. We use these measured properties to elucidate the governing array-scale transport mechanisms, which include the effects of morphology and energy carrier scattering from size effects and grain boundaries.

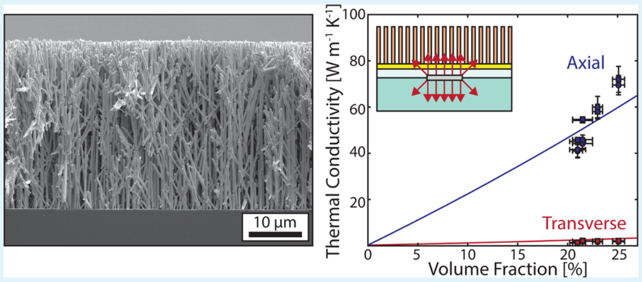

KEYWORDS: *copper nanowires, electrodeposition, nanocomposite, thermal interface material, thermal conductivity*

1. INTRODUCTION

There are a variety of applications for advanced materials that exhibit the unusual combination of high thermal conductivity and low mass density, such as in microelectronic packaging, thermal energy storage, and other energy conversion devices. For example, thermal interface materials (TIMs) require both high thermal conductivity and mechanical compliance for thermal management of high power density electronics. This combination of properties simultaneously achieves a low-resistance thermal pathway between devices and heat sinks while alleviating thermomechanical stresses that arise at the interface between dissimilar materials due to the mismatch in coefficients of thermal expansion. Advances in nanomaterials and composites have enabled conductive bulk materials, such as graphite and metals, to be nanostructured into a mechanically compliant geometry. In the past decade, this strategy has largely focused on aligned carbon nanotube (CNT) arrays and CNT-filled composites[1−3] due to the high thermal conductivity of individual CNTs[4,5] and the low elastic modulus of vertically aligned CNT arrays.[6,7] However, the high thermal conductivities of CNTs are closely linked to their microstructural quality and the matrix material. This has led to wide variations in the reported thermal conductivities of practical CNT arrays that may be associated with entanglement, defects, contact resistances, and damage incurred during processing.[8] In addition, demanding synthesis conditions pose challenges to scalability and device integration of CNT arrays.

Here we investigate the use of vertically aligned metal nanowire (NW) arrays and composites to preserve the high intrinsic thermal conductivity of the constituent metal while leveraging the mechanical compliance acquired through the high aspect ratio NWs. In thermal applications, metal NWs have been previously limited to use as unaligned filler particles in polymer matrices to produce a composite with a marginally increased effective thermal conductivity. Although many of these composites exhibit large enhancements in the effective thermal conductivity relative to the unfilled polymer matrix,[9] the magnitude of the thermal conductivity remains below 5 W m^{-1} K^{-1} because most composites are restricted to low filling fractions (<3%) of randomly oriented NWs.[10] In contrast, the effective thermal conductivity of a NW array or composite can be strongly increased by using a high density of NWs that are

Received: June 10, 2015
Accepted: August 18, 2015
Published: August 18, 2015

DOI: 10.1021/acsami.5b05147

aligned parallel to the heat flow. These aligned NW arrays can be fabricated using electrodeposition into sacrificial porous membranes,[11−13] which is an inexpensive, scalable, and tunable method to rapidly and controllably synthesize vertically aligned metal NWs over large areas. The porous membranes, which are commonly either anodized aluminum oxide (AAO)[11,14−26] or polycarbonate track-etched (PCTE) membranes,[12,27−41] are used as templates to confine metal deposition to the cylindrical pores, after which the membrane is dissolved. Many array-scale properties (e.g., conductivity, surface area-to-volume ratio) are derived from the geometry of the NWs in the array, which is determined by the membrane properties. Using this method, NWs can be synthesized with diameters ranging from ∼10 nm to ∼10 μm (determined by pore size), densities up to ∼50% (determined by pore density), and lengths up to ∼60 μm (limited by membrane thickness). Electrodeposited metal NW arrays have been utilized for applications including energy storage,[18] enhanced boiling surfaces,[21,23,24] and ultrasharp microscopy probe tips.[27,28]

Nearly all template-grown NWs in the literature are attached only to the membrane itself, where a thin (<1 μm) metal seed layer is either sputtered or evaporated onto the backside of the membrane to serve as a cathode from which the NWs are grown. In some instances, this thin seed layer is electrochemically thickened to provide mechanical stability to the base of the array. However, this membrane-only synthesis is only capable of producing self-supported NW arrays on thin foils, whereas many applications require the NWs to be directly attached to a separate device or substrate. As a result, efforts have been made to transfer these self-supported NW arrays onto substrates using bonding layers of indium solder[21] and silver-filled epoxy,[23] which leaves a residual bond line between the NWs and the substrate. For thermal applications, this bond line manifests as a parasitic interface resistance between the NW array and the adjacent surface. Direct synthesis of electrodeposited NWs onto a substrate is difficult using AAO and PCTE membranes because the membrane must remain in intimate contact with the underlying substrate during deposition. As a result, additional processing steps have been developed to achieve on-substrate synthesis using the membrane as a mask during metal deposition, where the membrane is held in place using either epoxy resin,[27,28] lithography-assisted template bonding,[39] or template adhesion by liquid film surface tension.[24] In this work, we present an electrostatic template adhesion technique used to directly synthesize vertically aligned copper NW arrays on centimeter-sized substrates, which eliminates any additional template bonding processes, intermediate bonding layers, or other parasitic thermal resistances. Furthermore, we introduce the use of direct current deposition with a sacrificial overplating layer to achieve 30 μm thick arrays of uniform NWs having <2% variation in length over the entire array.

Most metal NW transport measurements in the literature have been reported for individual NWs,[32,37,42] and there is minimal data available on array-scale transport properties. In one of the few contributions to array-scale characterization, Xu et al. used the laser flash technique to measure and extract an effective composite thermal conductivity of 30.3 W m^{-1} K^{-1} for a 9% dense film of self-supported electrodeposited silver nanowires embedded inside a PCTE membrane.[38] In the present work, we use the 3ω method, a frequency-domain electrothermal measurement technique, to measure both the axial and transverse components of the effective thermal conductivity of copper NW arrays. We implement this method by synthesizing the arrays directly onto substrates that contain electrically isolated metal heaters. The on-substrate NW synthesis provides a platform for both measuring intrinsic properties and also replicating a TIM application of aligned copper NWs. This method is applied to the array both while it remains embedded in the polycarbonate template and after dissolution of the template. In addition, we infiltrate a freestanding NW array with an organic phase change material and demonstrate the preservation of thermal properties after forming a new multifunctional composite.

2. EXPERIMENTAL SECTION

2.1. Copper Nanowire Synthesis. Copper NW arrays are synthesized using electrodeposition of copper into sacrificial porous templates. These templates are nominally 30 μm thick extruded PCTE membranes that contain randomly distributed hydrophilic (PVP-coated) pores of tunable diameter and number density (Sterlitech Corp.). Plan view scanning electron microscopy (SEM) images of each membrane are analyzed to measure the surface porosity and pore diameter of each membrane. After NW deposition, a cross-sectional SEM image is used to measure the resulting NW diameter and length, after which the total NW volume fraction is estimated using the pore number density and the NW diameter. A growth substrate is prepared by depositing a thin metal seed layer (5 nm Ti + 50 nm Au) onto the surface using electron beam evaporation; this serves as the electrodeposition cathode. The seed layer can be patterned using a shadow mask or photolithography to define specific regions of the substrate for NW growth.

The membrane is adhered to the substrate using a combination of the intrinsic electrostatic attraction and mechanical compression by a polytetrafluoroethylene (PTFE) aperture in the electrochemical cell (see Supporting Information). The membrane is placed on top of the substrate and rolled flat using a PTFE rod. The rolling is performed by pressing on top of the rod with moderate hand-applied pressure and rolling back and forth multiple times along the surface, beginning at a corner. During this time, the membrane turns from a mostly opaque white (before rolling) to a translucent gray (after flattening down). Multiple passes are required to fully roll out air pockets and wrinkles, which manifest as visible discolorations. The electrostatic attraction is sufficient to hold the membrane in place during normal handling of the substrate, but the PTFE aperture is required to protect the edges of the membrane from delamination. Without this additional edge protection, the membrane can peel away from the surface beginning at the edges when the hydrophilic membrane is immersed in water.

Potentiostatic electrodeposition is controlled using a potentiostat (Gamry Reference 600) and an all-PTFE, three-electrode electrochemical cell (see the Supporting Information). The counter electrode, reference electrode, and working electrode are composed of an oxygen-free copper plate (10 cm^2), a Ag/AgCl reference electrode (Bioanalytical Systems, Inc.), and the Au surface of the substrate beneath the membrane, respectively. A 50 mL aqueous acid−salt electrolyte bath consists of 0.6 M $CuSO_4$ (Sigma-Aldrich, >99%) to provide copper ions and 30 mM H_2SO_4 (Sigma-Aldrich, 95−98%) to increase the solution conductivity (pH 1.80 ± 0.03). Electrodeposition is performed in ambient air and at room temperature using an applied voltage of $V_{\text{applied}} = -120$ mV versus Ag/AgCl (corresponding to an overpotential $\eta = 200$ mV), during which the solution is magnetically stirred to minimize concentration gradients. After copper deposition, the overplating is removed by using tweezers to grab a corner of the film and slowly peeling upward. For a sufficiently thick overplating film, it remains cohesive during removal and peels off in a single, continuous piece of copper. Finally, the PCTE membrane is dissolved by immersing the substrate in dichloromethane (Sigma-Aldrich, >99%) for 1 h at 35 °C. The substrate with newly exposed NWs is then placed in deionized water, followed by ethanol, before being dried at room temperature in air.

Table 1. Summary of Geometric Properties of Vertically Aligned Copper NW Arrays Used in the Present Work Obtained Using Scanning Electron Microscopy

array ID	nominal pore diameter (nm)	surface porosity (%)	pore number density (pores/cm^2)	NW diameter (nm)	NW length (μm)	aspect ratio	estimated volume fraction (%)
1	200	7.6 ± 0.1	$(2.4 \pm 0.1) \times 10^8$	322 ± 6	31.6 ± 0.1	98 ± 2	19.5 ± 1.6
2	400	16.7 ± 0.8	$(1.3 \pm 0.1) \times 10^8$	466 ± 38	27.4 ± 0.2	59 ± 5	22.2 ± 5.7
3	1000	16.6 ± 0.2	$(2.1 \pm 0.1) \times 10^7$	1189 ± 45	28.7 ± 0.2	24 ± 1	23.3 ± 3.0

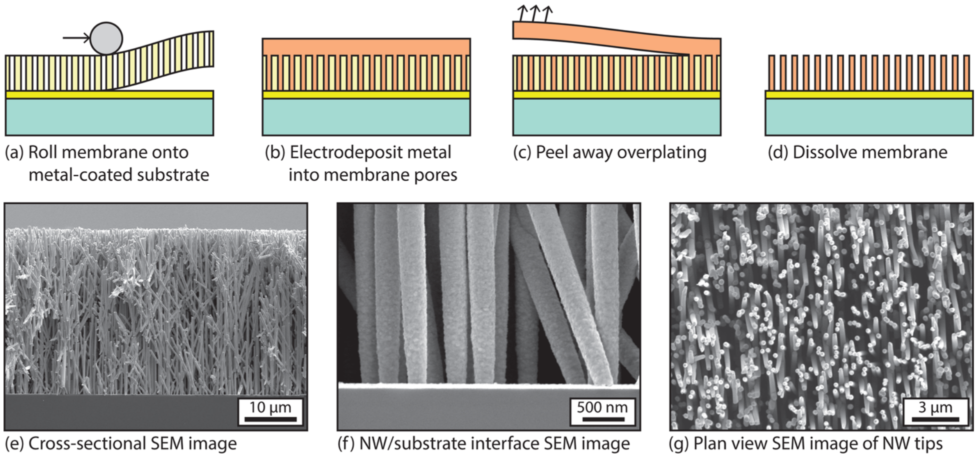

(a) Roll membrane onto metal-coated substrate
(b) Electrodeposit metal into membrane pores
(c) Peel away overplating
(d) Dissolve membrane
(e) Cross-sectional SEM image
(f) NW/substrate interface SEM image
(g) Plan view SEM image of NW tips

Figure 1. Vertically aligned metal NWs are grown directly onto substrates using template-assisted electrodeposition. (a) A porous membrane is rolled onto a gold-coated substrate and (b) is used as a mask during electrodeposition to form metal nanowires. Electrodeposition is continued until all pores are entirely filled and a continuous, solid metal film forms on the top of the membrane; this ensures nanowire uniformity over the entirety of the array. (c) The overplated film is then peeled away from the NW-filled membrane. (d) The membrane is dissolved to yield a freestanding NW array. (e) A cross-sectional SEM image of a copper NW array shows the preferential vertical alignment and the uniformity of the array. (f) A high-magnification SEM image of the NW/substrate interface shows the tapered ends of the individual NWs and demonstrates the absence of any intermediate layer between the base of the NWs and the metal seed layer on the substrate. (g) A plan view SEM image shows the NW packing density and array surface morphology.

The interstitial volume of a NW array is infiltrated via capillary action with an organic phase change material (see the Supporting Information). A ~1 mg piece of solid paraffin wax (Sigma-Aldrich, melting temperature = 53−57 °C) is placed at the edge of a freestanding NW array at room temperature. The substrate is then placed on a hot plate at 75 °C, and the paraffin wax melts and wicks into the interstitial volume between the NWs. Upon removal from the heat, the paraffin wax solidifies and encapsulates the NW array.

2.2. Thermal Characterization. The 3ω method is implemented using microfabricated devices composed of a fused silica wafer with photolithographically patterned metal heater lines having a nominal length of 1000 μm and a nominal width of 5 μm deposited by electron beam evaporation (5 nm Ti + 60 nm Pt). These heater lines are patterned into a four-point probe configuration, and the entire device is passivated using a thermally thin SiO_2 film. It is critical to achieve full passivation of these devices to prevent current leakage through the high-conductivity metal samples deposited above the heater lines. To achieve complete electrical isolation, we incorporated a 250 nm thick SiO_2 trilayer passivation film. This passivation stack consists of 40 nm of SiO_2 deposited by atomic layer deposition (ALD) to conformally coat the patterned metal features, 170 nm of SiO_2 deposited by high-density plasma-enhanced chemical vapor deposition to thicken the film for mechanical stability during thermal expansion of the underlying metal, and an additional 40 nm of SiO_2 deposited by ALD to patch any remaining pinholes or other defects.

Each device is first calibrated prior to seed layer evaporation and NW deposition using a temperature-controlled vacuum chamber to measure the linear relationship between temperature and resistance in the metal heater lines (see the Supporting Information). The heaters used in this work have resistances that range from 450 to 500 Ω and sensitivities that range from $dR/dT = 1.22$ to 1.34 Ω K^{-1}. Next, the 3ω method is used to characterize the heater line half-width b and the thermal conductivity and heat capacity of the fused silica substrate, which are found to be $k_{FS} = 1.29 \pm 0.01$ W m^{-1} K^{-1} and $C_{v,FS} = (1.67 \pm 0.01) \times 10^6$ J m^{-3} K^{-1}, respectively. The metal seed layer (5 nm Ti + 50 nm Au) is then deposited using electron beam evaporation through a shadow mask having a 3 mm diameter circular aperture onto the center of the device. The seed layer is centered above the exposed window of the buried working electrode lead, which provides electrical continuity for electrodeposition. A second 3ω calibration is used to measure the effective thermal conductivity of the composite metal seed layer on each device, which ranges from 102 to 120 W m^{-1} K^{-1}. Finally, the NW array is synthesized above the metal seed layer by attaching the template to the substrate and using the electrochemical cell to provide current to the buried working electrode during electrodeposition. The presence of underlying patterns is not observed to affect the ability to form intimate contact between the pliable membrane and the substrate because the metal lines have low aspect ratios and are covered with a passivation layer and a metal seed layer that smooth out the surface topography.

The thermal properties of each NW array are first measured while the NWs are embedded in the PCTE membrane and are measured again after the membrane is dissolved to form a freestanding NW array. A multiparameter fit of eq 2a,b to the experimental data of eq 1 is applied to the freestanding array to simultaneously extract the axial thermal conductivity $k_{\|}$, the transverse thermal conductivity $k_{\perp}$, and the effective heat capacity of the array $C_{v,eff}$. The NW volume fraction, $0 \leq \Phi \leq 1$, is determined from $C_{v,eff}$, which for an effective medium is approximately given by the volume fraction-scaled heat capacity of the bulk copper, $C_{v,Cu}$, such that $C_{v,eff} = C_{v,Cu}\Phi$. After extracting Φ for each freestanding array, we next fit the data for the NW/polycarbonate composite to extract the effective thermal conductivity of the composite. This two-component composite is composed of metal NW fillers embedded in a polycarbonate matrix and modeled as an effective medium, where the effective heat capacity is again equal to the volume fraction-weighted average of the two components such that

$C_{v,\mathrm{eff}} = C_{v,\mathrm{Cu}}\Phi + C_{v,\mathrm{PC}}(1 - \Phi)$. This assumption reduces the analysis for the NWs embedded in the membrane to two fitting parameters, $k_{\parallel}$ and $k_{\perp}$.

3. RESULTS AND DISCUSSION

Copper NW arrays are synthesized using templated electrodeposition, where a sacrificial PCTE porous membrane (see Table 1) is used to mask a substrate while copper is electrochemically deposited into the pores. These pores are generally cylindrical and taper near the opening such that the pore diameter at the membrane surface is smaller than the diameter in the center. The membrane is rolled onto a metal-coated substrate using a polytetrafluoroethylene (PTFE) rod to remove wrinkles and air gaps as shown in Figure 1a. The membrane electrostatically adheres to the gold seed layer, which enables NW growth from the substrate surface with no intermediate transition layer or bond line. The membrane-masked substrate is sealed into an aperture assembly that is used to define the area of electrodeposition, and the exposed area (0.07 cm^2) is saturated with the electrolyte solution for several minutes to ensure uniform pore wetting prior to deposition. The aperture assembly is inserted into a three-electrode electrochemical cell (see the Supporting Information), and an isolated metal pad electrically contacts the cathode on the outer edge of the substrate.

Potentiostatic electrodeposition is used to deposit copper into the membrane pores beginning at the substrate as shown in Figure 1b. Because electrodeposition is a Faradaic process, the deposition time is correlated to the array height (i.e., nanowire length), and different regimes in the current versus time characteristic are indicative of the extent of NW growth[12,15,33,41,43] as shown in Figure 2. During stage I, the pores begin to fill with metal, forming the individual NWs. Once the pores are entirely filled with copper, metal begins to deposit isotropically from the NW tips during stage II, forming mushroom-like caps. When the caps become sufficiently large, they coalesce into a single, continuous planar film during stage III that grows above the membrane. To calibrate the NW growth rate, copper is deposited for different deposition times within stage I, and the resulting array height is measured using cross-sectional SEM imaging. However, each pore experiences small differences in the metal deposition rate due to diffusion limitations of direct current electrodeposition. This causes the dispersion in NW length to increase with deposition time, leading to a high degree of surface roughness across the array during stage I growth. This diffusion-limited growth can be mitigated through pulsed electrodeposition to provide a more uniform NW growth rate,[18] which requires careful calibration and tuning of the electrochemistry and deposition parameters. Instead, we use direct current electrodeposition of copper into stage III growth such that all of the pores are entirely filled and a continuous copper overplating film remains on the membrane surface.

After the copper deposition, the substrate is immersed in DI water to remove the excess electrolyte. The overplating film is peeled away from the top surface, separating from the tips of the NWs as shown in Figure 1c, while the NWs remain embedded in the membrane to preserve the array morphology. By depositing a sufficiently thick overplating layer, the planar film remains cohesive during removal and separates as a single, continuous piece. This process results in a NW array with deviation in surface planarity (i.e., variation in array thickness or NW length) of approximately 1%. The substrate is then immersed in dichloromethane to dissolve the polycarbonate membrane. The PCTE membrane templates used in this work have nominal pore diameters of 200, 400, and 1000 nm and a nominal thickness of 30 μm, and the corresponding NW arrays are shown in Figure 3.

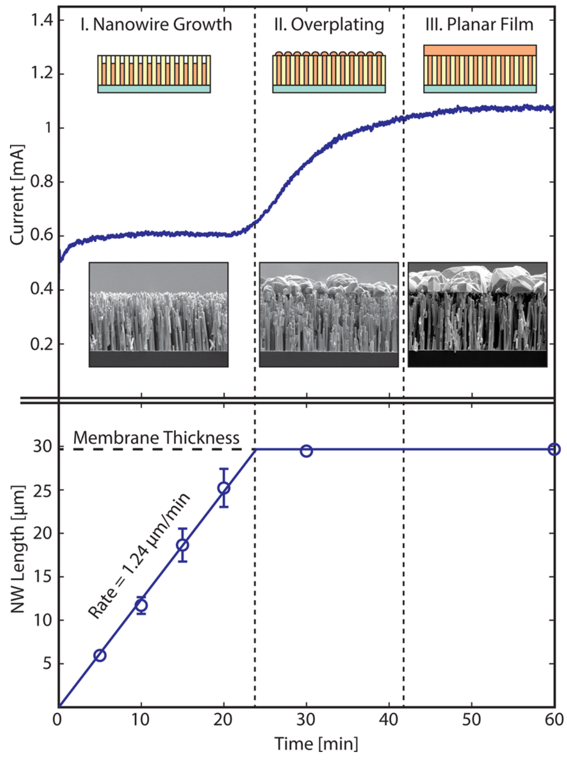

Figure 2. Representative current versus time characteristic for potentiostatic electrodeposition of copper NWs and the corresponding NW array growth rate curve as measured using cross-sectional SEM images. Three distinct stages are identified in the characteristic current response. During stage I, electrodeposition is confined to only the pores of the membrane, resulting in a reduced current and a linear relationship between nanowire length (i.e., array height) and time. During stage II, the pores begin to fill completely with metal and caps form on the surface of the membrane, beginning at the tips of the nanowires. Eventually the caps become large enough to coalesce and merge into a solid copper film of constant surface area during stage III, resulting in a constant current with planar film growth on the surface.

The effective thermal conductivity of each NW array is measured using the 3ω method, which is well-described in the literature.[44−48] In brief, the 3ω method utilizes a single patterned metal line driven by a current source at frequency ω to provide Joule heating and subsequent temperature oscillations at a frequency of 2ω. Due to the temperature coefficient of resistance of the metal, the resistance of the line is also perturbed at a frequency of 2ω, leading to an overall voltage oscillation at a frequency of 3ω, which is detected using a lock-in amplifier. We implement this measurement by growing the NW array directly above an electrically isolated metal line that is used simultaneously as both a heater and a thermometer. The device design is derived from a structure originally employed by Roy-Panzer et al. for use in high-sensitivity thermal characterization of fluid microdroplets[49] and is adapted to contain a buried electrode to facilitate electrodeposition onto the center of the device[50] as shown in Figure 4.

In each 3ω measurement, the spatially averaged temperature rise in the heater ΔT is mapped to the measured $V_{3\omega}$ signal[44]

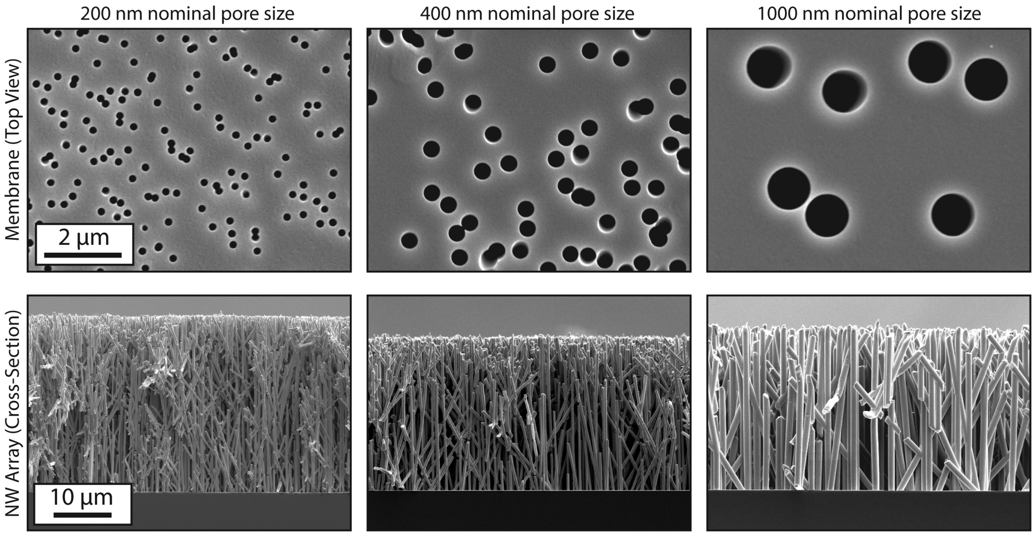

Figure 3. (Top) Plan view SEM images of polycarbonate track-etched membranes and (bottom) cross-sectional SEM images of the resulting nanowire arrays synthesized on silicon substrates.

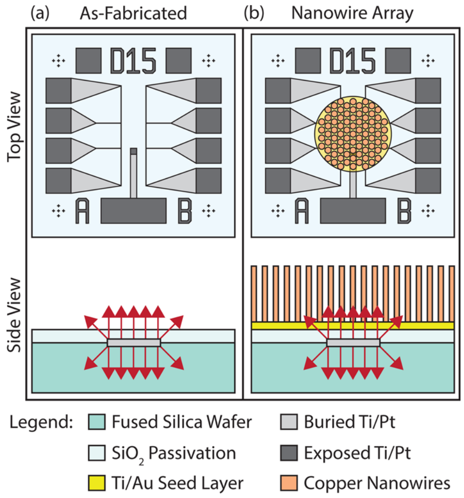

Figure 4. Top and side views of an electrothermal measurement device (a) before and (b) after metal seed layer deposition and nanowire growth. Each device contains two buried heater lines, and an additional metal line connects to the center of the device to conduct current during electrodeposition. The Ti/Au seed layer is evaporated through a shadow mask over the center of the device, and nanowires are grown directly onto this seed layer.

$$\Delta T = \frac{2V_{3\omega}\frac{\mathrm{d}T}{\mathrm{d}R}}{I_{\mathrm{RMS}}} \tag{1}$$

where $\mathrm{d}T/\mathrm{d}R$ is the measured linear relationship between temperature and resistance in the metal line and I_{RMS} is the root-mean-squared electrical current. The $V_{3\omega}$ signal is recorded over a selected frequency range of 200−6000 Hz and converted to a thermal frequency response $\Delta T(\omega)$ using eq 1. The thermal properties of the multilayered stack shown in Figure 4 are extracted by using a least-squares fitting algorithm to fit the amplitude of the measured frequency-domain thermal response to the analytical heat diffusion equation in stratified media given by eq 2a,b.[44,45,51,52] The spatially averaged temperature rise ΔT at the location of heating for a defined multilayered system can be derived[45,52] as

$$\Delta T = \frac{P}{2\pi L b^2}\int_0^\infty \frac{B^+(m) + B^-(m)}{A^+(m)B^-(m) - A^-(m)B^+(m)} \times \frac{\sin^2(mb)}{\gamma_j m^2}\,\mathrm{d}m \tag{2a}$$

$$\gamma_j = k_j\sqrt{\eta_j m^2 - i\frac{\omega}{\alpha_j}} \tag{2b}$$

where P is the heating power, L and b are the length and half-width of the heater, respectively, k_j and α_j are the thermal conductivity and diffusivity of the jth layer, η_j is the anisotropy ratio of the jth layer (i.e., the ratio of the in-plane to cross-plane thermal conductivity), and A and B are dimensionless parameters solved using a recursive matrix method. In this model, the 250 nm thick SiO_2 passivation layer, the 55 nm thick metal seed layer, and the NW array are treated as discrete layers having finite thickness because the thermal penetration length is greater than the layer thickness over the measurement frequency range. The fused silica substrate and air above the sample are treated as semi-infinite media.

This method is validated by measuring the thermal conductivity of a solid electrodeposited copper film having a thickness of 4.9 ± 0.1 μm. The heat capacity is fixed at the bulk value of $C_{\mathrm{v,Cu}} = 3.44 \times 10^6$ J m^{-3} K^{-1}, and the resulting thermal conductivity is measured to be $k_{\mathrm{Cu}} = 383 \pm 6$ W m^{-1} K^{-1}. This conductivity is nearly equal to the value for single-crystal bulk copper[53] ($k_{\mathrm{Cu,SC}}$ = 398 W m^{-1} K^{-1} at 300 K). Because electrodeposition is capable of producing metals ranging from dendritic to fully densified and having microstructures ranging from nanocrystalline to large single crystals, the measured thermal conductivity suggests that the electrodeposited copper in the present work is fully densified and polycrystalline with large grains. Grain boundary scattering of electrons in metals is well described by Mayadas and Shatzkes[54] using a semi-empirical correlation between electron transport and grain size given by

$$\frac{k_{\mathrm{Cu}}}{k_{\mathrm{Cu,SC}}} = 1 - \frac{3}{2}\alpha + 3\alpha^2 - 3\alpha^3 \ln\left(1 + \frac{1}{\alpha}\right) \tag{3a}$$

$$\alpha = \frac{\lambda}{D_{\mathrm{GB}}}\frac{R}{(1-R)} \tag{3b}$$

where D_{GB} is the average grain size, λ is the mean free path of conduction electrons in bulk metal, and R is a reflection coefficient for electrons at grain boundaries. For copper, $\lambda \approx 39$ nm at room temperature and the reflection coefficient is $R \approx 0.24$,[54] which corresponds to an average grain size of approximately 300−600 nm for the electrodeposited copper film. We confirm that the grain sizes in the electrodeposited copper are on the order of $\sim 10^2$ nm using transmission electron microscopy (see the Supporting Information).

Each copper NW array is synthesized on a microfabricated substrate, and the thermal properties of the array are measured both while the NWs are embedded in the membrane and again after the membrane is dissolved. The thermal conductivity is found to be highly anisotropic due to the preferential vertical alignment of the NWs. Cross-plane conduction is primarily facilitated by axial transport along the NWs, whereas in-plane conduction is limited by serial resistances composed of the insulating matrix and contact resistances between adjacent NWs and the matrix. Consequently, the axial thermal conductivity $k_{\|}$ (i.e., parallel to the NWs) is observed to be more than an order of magnitude larger than the transverse thermal conductivity $k_{\perp}$ (i.e., perpendicular to the NWs) with anisotropy ratios $\eta = k_{\|}/k_{\perp}$ as high as 40. For the 21−25% dense freestanding NW arrays developed in this work, we measure effective thermal conductivity values of $k_{\|} = 41$−70 W m^{-1} K^{-1} and $k_{\perp} = 1.1$−2.0 W m^{-1} K^{-1}. For the NWs embedded in the polycarbonate membrane, we observe thermal conductivities of $k_{\|} = 45$−72 W m^{-1} K^{-1} and $k_{\perp} = 1.3$−2.2 W m^{-1} K^{-1}. Because axial conduction in the array primarily occurs along the copper NWs rather than the interstitial matrix, we observe only a minor decrease in $k_{\|}$ between the initial NWs embedded in polycarbonate and the freestanding array after membrane dissolution. In addition, the transverse conduction is limited by series resistances between the NWs and the matrix, and we observe a consistent decrease in $k_{\perp}$ by ~0.25 W m^{-1} K^{-1} across all samples after replacing the polycarbonate matrix with air. These effects are further obfuscated by the potential for irreversible morphological changes that may occur during the membrane dissolution process. While embedded in the membrane, the individual NWs are constrained to their as-synthesized alignment and morphology. During the dissolution and subsequent drying processes, the now-unsupported and flexible NWs may deform and alter the array morphology to favor more isotropic conduction. This is supported by observing that the fractional reduction in $k_{\|}$ between freestanding NWs and composite NWs increases with aspect ratio (AR). For the 322 nm diameter NWs (AR = 98), there is a 17% average reduction in $k_{\|}$, whereas the 466 nm diameter NWs (AR = 59) experience only a 9% average reduction in $k_{\|}$. The 1189 nm diameter NWs (AR = 24) experience a negligible change in $k_{\|}$ that is within the uncertainty of the measurement.

Additional functionality can be provided to the array by infiltrating the available interstitial volume with a functional material. For example, infiltration with polymers (e.g., epoxy, PDMS) can provide mechanical and chemical stability, infiltration with eutectics (e.g., AuSn) can enhance the effective conductivity, and infiltration with phase-change materials (e.g., paraffin wax) can give the NW composite a high effective thermal capacitance. We demonstrate the ability to infiltrate a freestanding NW array with paraffin wax, which provides additional thermal capacitance to the array to buffer thermal transients in microelectronics applications, and we observe retention of the effective composite thermal conductivity. For as-synthesized 466 nm diameter NWs embedded in the PCTE membrane ($k_{\mathrm{polycarbonate}} = 0.2$ W m^{-1} K^{-1}), we first measure $k_{\|} = 45.1 \pm 1.0$ W m^{-1} K^{-1} and $k_{\perp} = 1.34 \pm 0.04$ W m^{-1} K^{-1}. After membrane dissolution, these values are reduced to $k_{\|} = 41.6 \pm 3.6$ W m^{-1} K^{-1} and $k_{\perp} = 1.18 \pm 0.02$ W m^{-1} K^{-1}. However, after infiltrating the array with paraffin wax ($k_{\mathrm{paraffin}} = 0.24$ W m^{-1} K^{-1}), we observe a recovery of the effective axial thermal conductivity of the composite NW array to $k_{\|} = 43.4 \pm 1.0$ W m^{-1} K^{-1}. This suggests that there are minor contributions both from morphological changes during matrix removal and matrix infiltration (irreversible changes) and from the thermal bridge provided by the matrix material between adjacent NWs (reversible changes). We also recover the transverse thermal conductivity to $k_{\perp} = 1.37 \pm 0.05$ W m^{-1} K^{-1} after paraffin wax infiltration. This confirms the expectation that the contribution of the matrix is significant to the transverse conductivity because the lateral conduction pathway consists of series resistances that are limited by the thermal resistivity of the matrix.

The effective transport properties of a binary composite can be interpreted using a compositional phase diagram because the conductivity is a function of both the composite morphology (i.e., the effective transport path length in each phase) and the composite composition (i.e., the available fractional contribution from the individual components). In the diffusive limit for thermal conduction where one component has a negligible thermal conductivity compared to the other (e.g., $k_{\mathrm{Cu}} \gg k_{\mathrm{air}}$), the upper bound of the effective axial thermal conductivity of the composite $k_{\|,\max}$ scales linearly with the volume fraction, Φ:

$$k_{\|,\max} = k_{\mathrm{Cu}}\Phi \tag{4}$$

This is equivalent to modeling the two components as noninteracting parallel resistors where each NW exhibits bulk-like thermal conductivity and the alignment minimizes the effective conduction path length. However, measured values of $k_{\|}$ are reduced below $k_{\|,\max}$ due to both internal mechanisms, including grain boundary and surface scattering of energy carriers, and morphological mechanisms, including defects in the individual NWs and tortuosity and entanglement that increase the effective heat transfer path length.

The array morphology is likely the primary source of the reduced effective thermal conductivity due to deviations from the nominal vertical alignment of the NWs. As the NW aspect ratio (i.e., flexibility) increases, these morphological imperfections may become increasingly prominent due to additional NW entanglement and tortuosity. Effective medium theory (EMT) is a well-established methodology for predicting the effective transport properties of composite media based on both composition and morphology. We apply a general EMT framework for the axial and transverse thermal conductivities developed by Nan et al.[55] that has been previously applied to aligned[3] and unaligned[56] CNT composites. The NW alignment factor, $\langle\cos^2\theta\rangle$, varies from 0.33 for randomly oriented NWs to 1 for perfectly collimated NWs. We use cross-sectional SEM images to measure an alignment factor of 0.93 ± 0.02 for all arrays in this work, although this is difficult to estimate because the NWs along the cleaving plane are necessarily disturbed while the cross-section is prepared (see the Supporting Information). Although this model can fully consider the thermal boundary resistance between the NWs and matrix, we neglect this boundary effect because it is small compared to the volumetric resistance of the insulating matrix material. When scaled with Φ, this model predicts a reduction in $k_{\parallel}$ that is comparable to the measured data and also accurately captures the low observed values of $k_{\perp}$ for high aspect ratio NWs as shown in Figure 5a.

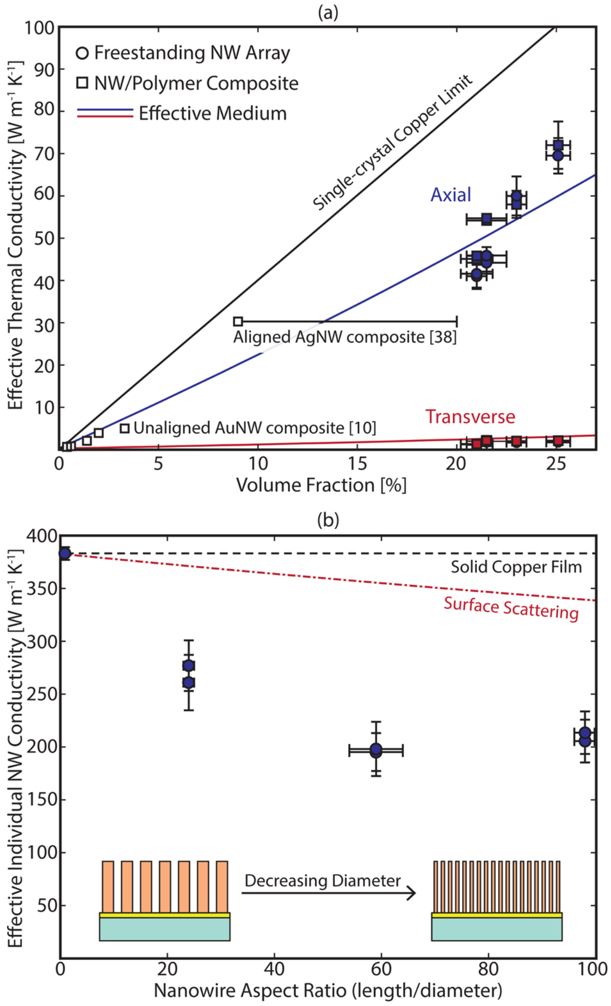

Figure 5. (a) The effective thermal conductivity of the NW arrays is shown as a function of the volume fraction, including the axial thermal conductivity $k_{\parallel}$ (blue) and $k_{\perp}$ (red) for NWs embedded in the polycarbonate membrane (squares) and as freestanding arrays (circles). Whereas axial thermal conductivity scales with the density of NWs, the transverse thermal conductivity is limited by the large resistance contribution from the interstitial volume and remains constant with volume fraction. The upper bound for thermal conductivity is given using eq 4 for single-crystal copper (black line). The effects of morphology are modeled using effective medium theory (blue and red lines), which shows a comparable reduction in axial conductivity as observed experimentally and also agrees with the measured transverse thermal conductivity values. Data are also shown for metal NW composites in the literature, including unaligned Au NWs randomly dispersed in PDMS[10] and for aligned Ag NWs embedded in a PCTE membrane.[38] (b) The effective thermal conductivity per NW, k_{ind}, is calculated from eq 5 and is reduced from the bulk thermal conductivity of electrodeposited copper (black line). Size effects and surface scattering contribute to a fraction of this reduction (red line), which becomes increasingly significant as the NW diameter decreases. The effects of grain boundary scattering likely also increase with a reduced NW diameter.[57]

We can rewrite eq 4 to define an effective thermal conductivity for an individual NW k_{ind} as

$$k_{\text{ind}} = \frac{k_{\parallel}}{\Phi} \tag{5}$$

For freestanding NW arrays, this leads to k_{ind} = 195−277 W m^{-1} K^{-1} for the NW arrays in the present work, which represents a suppression of the magnitude to ∼50−75% of the bulk conductivity of copper. Internal scattering mechanisms, including surface scattering and grain boundary scattering, likely contribute to this reduction in k_{ind}. The surface scattering-limited individual NW conductivity $k_{\text{ind,surf}}$ can be estimated using Matthiessen's rule as a scaling argument

$$k_{\text{ind,surf}} = \frac{D}{D + \lambda} k_{\text{ind}} \tag{6}$$

where λ is the bulk electron mean free path and D is the diameter of the NW as used to estimate the surface-limited mean free path. For the smallest NWs used in the present work (D = 322 nm), surface scattering is estimated to only suppress $k_{\text{ind,surf}}$ to ∼89% of k_{ind}. Alternatively, the grain size in the copper NWs may be reduced relative to the bulk copper film, and grain boundary scattering may account for the majority of the suppression in k_{ind}. For example, Völklein et al. measured the thermal conductivity of an individual electrodeposited platinum NW (D = 131 nm) and observed a reduction in conductivity to only ∼29% of the bulk value, which is attributed to grain boundary scattering rather than size effects.[37] Kim et al. further demonstrated the impact of grain boundary structure on electron scattering in electrodeposited copper NWs and observed that grain size tends to scale linearly with geometric dimension.[57] This suggests that while the grain size in bulk copper is observed to be much larger than λ, transport in the individual NWs is expected to become increasingly impeded by grain boundaries with shrinking NW diameter. The combination of array-scale morphology with enhanced scattering within the constituent NWs leads to effective transport properties that are reduced below the diffusive upper limit.

4. CONCLUSIONS

We have demonstrated a facile method to synthesize and integrate highly uniform arrays of metal nanowires on substrates and devices that does not require an additional bonding layer for either the template or the NW array. This method brings the high thermal conductivity NW array adjacent to active devices and other heat sources for high heat flux thermal management applications. Although the direct on-substrate synthesis minimizes one-interface resistance and the high conductivity NWs reduce the volumetric resistance, it will be necessary to develop a method to bond the tips of the NWs to an adjacent substrate (e.g., a heat sink) to reduce contact resistance. We present both the effective axial and transverse thermal conductivities of freestanding copper NW arrays and report values as large as 70 W m^{-1} K^{-1}. Such metal NW composites, whether embedded in the growth template, left as a freestanding array, or infiltrated with a functional matrix material, offer multifunctionality without compromising the stability or intrinsic advantage of the high-conductivity NWs.

■ ASSOCIATED CONTENT

Supporting Information

The Supporting Information is available free of charge on the ACS Publications website at DOI: 10.1021/acsami.5b05147.

> Electrochemical cell and electrodeposition properties, polymer infiltration methodology, fabrication and calibration of measurement devices, measurement sensitivity and uncertainty analyses, tabulated thermal conductivity data, and effective medium theory model (PDF)

■ AUTHOR INFORMATION

Corresponding Author

*(K.E.G.) E-mail: goodson@stanford.edu.

Notes

The authors declare no competing financial interest.

■ ACKNOWLEDGMENTS

We gratefully acknowledge financial support from the NSF/DOE Partnership on Thermoelectric Devices for Vehicle Applications (Grant 1048796) and a Northrop Grumman Aerospace Systems grant. M.T.B. and T.S.E. acknowledge government support under and awarded by the U.S. Department of Defense, Air Force Office of Scientific Research, National Defense Science and Engineering Graduate (NDSEG) Fellowship, 32 CFR 168a. S.R.-P. and T.S.E. gratefully acknowledge the support of the National Science Foundation Graduate Research Fellowship Program. We performed this work in part at the Stanford Nanofabrication Facility, which is supported by the NSF through the National Nanotechnology Infrastructure Network. We are also grateful for technical discussions with A. Sood and C. Coyan and for microfabrication support from W. Park and K. Chang.

■ REFERENCES

(1) Tong, T.; Yang, Z.; Delzeit, L.; Kashani, A.; Meyyappan, M.; Majumdar, A. Dense Vertically Aligned Multiwalled Carbon Nanotube Arrays as Thermal Interface Materials. *IEEE Trans. Compon. Packag. Technol.* **2007**, *30*, 92−100.

(2) Cross, R.; Cola, B. A.; Fisher, T.; Xu, X.; Gall, K.; Graham, S. A Metallization and Bonding Approach for High Performance Carbon Nanotube Thermal Interface Materials. *Nanotechnology* **2010**, *21*, 445705.

(3) Marconnet, A. M.; Yamamoto, N.; Panzer, M. A.; Wardle, B. L.; Goodson, K. E. Thermal Conduction in Aligned Carbon Nanotube-Polymer Nanocomposites with High Packing Density. *ACS Nano* **2011**, *5*, 4818−4825.

(4) Pop, E.; Mann, D.; Wang, Q.; Goodson, K. E.; Dai, H. Thermal Conductance of an Individual Single-Wall Carbon Nanotube above Room Temperature. *Nano Lett.* **2006**, *6*, 96−100.

(5) Pettes, M. T.; Shi, L. Thermal and Structural Characterizations of Individual Single-, Double-, and Multi-Walled Carbon Nanotubes. *Adv. Funct. Mater.* **2009**, *19*, 3918−3925.

(6) Gao, Y.; Kodama, T.; Won, Y.; Dogbe, S.; Pan, L.; Goodson, K. E. Impact of Nanotube Density and Alignment on the Elastic Modulus near the Top and Base Surfaces of Aligned Multi-Walled Carbon Nanotube Films. *Carbon* **2012**, *50*, 3789−3798.

(7) Won, Y.; Gao, Y.; Panzer, M. A.; Dogbe, S.; Pan, L.; Kenny, T. W.; Goodson, K. E. Mechanical Characterization of Aligned Multi-Walled Carbon Nanotube Films Using Microfabricated Resonators. *Carbon* **2012**, *50*, 347−355.

(8) Marconnet, A. M.; Panzer, M. A.; Goodson, K. E. Thermal Conduction Phenomena in Carbon Nanotubes and Related Nanostructured Materials. *Rev. Mod. Phys.* **2013**, *85*, 1295−1326.

(9) Wang, S.; Cheng, Y.; Wang, R.; Sun, J.; Gao, L. Highly Thermal Conductive Copper Nanowire Composites with Ultralow Loading: Toward Applications as Thermal Interface Materials. *ACS Appl. Mater. Interfaces* **2014**, *6*, 6481−6.

(10) Balachander, N.; Seshadri, I.; Mehta, R. J.; Schadler, L. S.; Borca-Tasciuc, T.; Keblinski, P.; Ramanath, G. Nanowire-Filled Polymer Composites with Ultrahigh Thermal Conductivity. *Appl. Phys. Lett.* **2013**, *102*, 093117.

(11) Brumlik, C. J.; Martin, C. R. Template Synthesis of Metal Microtubules. *J. Am. Chem. Soc.* **1991**, *113*, 3174−3175.

(12) Whitney, T. M.; Searson, P. C.; Jiang, J. S.; Chien, C. L. Fabrication and Magnetic Properties of Arrays of Metallic Nanowires. *Science* **1993**, *261*, 1316−1319.

(13) Toimil-Molares, M. E. Characterization and Properties of Micro- and Nanowires of Controlled Size, Composition, and Geometry Fabricated by Electrodeposition and Ion-Track Technology. *Beilstein J. Nanotechnol.* **2012**, *3*, 860−83.

(14) Yin, A. J.; Li, J.; Jian, W.; Bennett, A. J.; Xu, J. M. Fabrication of Highly Ordered Metallic Nanowire Arrays by Electrodeposition. *Appl. Phys. Lett.* **2001**, *79*, 1039.

(15) Riveros, G.; Gómez, H.; Cortes, A.; Marotti, R. E.; Dalchiele, E. A. Crystallographically-Oriented Single-Crystalline Copper Nanowire Arrays Electrochemically Grown into Nanoporous Anodic Alumina Templates. *Appl. Phys. A: Mater. Sci. Process.* **2005**, *81*, 17−24.

(16) Cao, H.; Wang, L.; Qiu, Y.; Zhang, L. Synthesis and I−V Properties of Aligned Copper Nanowires. *Nanotechnology* **2006**, *17*, 1736−1739.

(17) Kline, T. R.; Tian, M.; Wang, J.; Sen, A.; Chan, M. W. H.; Mallouk, T. E. Template-Grown Metal Nanowires. *Inorg. Chem.* **2006**, *45*, 7555−7565.

(18) Taberna, P. L.; Mitra, S.; Poizot, P.; Simon, P.; Tarascon, J. M. High Rate Capabilities Fe3O4-Based Cu Nano-Architectured Electrodes for Lithium-Ion Battery Applications. *Nat. Mater.* **2006**, *5*, 567−73.

(19) Cao, G.; Liu, D. Template-Based Synthesis of Nanorod, Nanowire, and Nanotube Arrays. *Adv. Colloid Interface Sci.* **2008**, *136*, 45−64.

(20) Inguanta, R.; Piazza, S.; Sunseri, C. Novel Procedure for the Template Synthesis of Metal Nanostructures. *Electrochem. Commun.* **2008**, *10*, 506−509.

(21) Chen, R.; Lu, M. C.; Srinivasan, V.; Wang, Z.; Cho, H. H.; Majumdar, A. Nanowires for Enhanced Boiling Heat Transfer. *Nano Lett.* **2009**, *9*, 548−53.

(22) Thongmee, S.; Pang, H. L.; Ding, J.; Lin, J. Y. Fabrication and Magnetic Properties of Metallic Nanowires via AAO Templates. *J. Magn. Magn. Mater.* **2009**, *321*, 2712−2716.

(23) Im, Y.; Joshi, Y.; Dietz, C.; Lee, S. S. Enhanced Boiling of a Dielectric Liquid on Copper Nanowire Surfaces. *Int. J. Micro-Nano Scale Transp.* **2010**, *1*, 79−95.

(24) Yao, Z.; Lu, Y.-W.; Kandlikar, S. G. Direct Growth of Copper Nanowires on a Substrate for Boiling Applications. *Micro Nano Lett.* **2011**, *6*, 563.

(25) Tan, M.; Chen, X. Growth Mechanism of Single Crystal Nanowires of FCC Metals (Ag, Cu, Ni) and hcp Metal (Co) Electrodeposited. *J. Electrochem. Soc.* **2012**, *159*, K15.

(26) Zaraska, L.; Sulka, G. D.; Jaskuła, M. Fabrication of Free-Standing Copper Foils Covered with Highly-Ordered Copper Nanowire Arrays. *Appl. Surf. Sci.* **2012**, *258*, 7781−7786.

(27) Motoyama, M.; Dasgupta, N. P.; Prinz, F. B. Electrochemical Deposition of Metallic Nanowires as a Scanning Probe Tip. *J. Electrochem. Soc.* **2009**, *156*, D431−D438.

(28) Motoyama, M.; Prinz, F. B. Electrodeposition and Behavior of Single Metal Nanowire Probes. *ACS Nano* **2014**, *8*, 3556−3566.

(29) Motoyama, M.; Fukunaka, Y.; Sakka, T.; Ogata, Y. H.; Kikuchi, S. Electrochemical Processing of Cu and Ni Nanowire Arrays. *J. Electroanal. Chem.* **2005**, *584*, 84−91.

(30) Schönenberger, C.; van der Zande, B. M. I.; Fokkink, L. G. J.; Henny, M.; Schmid, C.; Krüger, M.; Bachtold, A.; Huber, R.; Birk, H.; Staufer, U. Template Synthesis of Nanowires in Porous Polycarbonate

Membranes: Electrochemistry and Morphology. *J. Phys. Chem. B* **1997**, *101*, 5497−5505.

(31) Enculescu, I.; Siwy, Z.; Dobrev, D.; Trautmann, C.; Toimil Molares, M. E.; Neumann, R.; Hjort, K.; Westerberg, L.; Spohr, R. Copper Nanowires Electrodeposited in Etched Single-Ion Track Templates. *Appl. Phys. A: Mater. Sci. Process.* **2003**, *77*, 751−755.

(32) Toimil Molares, M. E.; Höhberger, E. M.; Schaeflein, C.; Blick, R. H.; Neumann, R.; Trautmann, C. Electrical Characterization of Electrochemically Grown Single Copper Nanowires. *Appl. Phys. Lett.* **2003**, *82*, 2139.

(33) Konishi, Y.; Motoyama, M.; Matsushima, H.; Fukunaka, Y.; Ishii, R.; Ito, Y. Electrodeposition of Cu Nanowire Arrays with a Template. *J. Electroanal. Chem.* **2003**, *559*, 149−153.

(34) Schuchert, I. U.; Molares, M. E. T.; Dobrev, D.; Vetter, J.; Neumann, R.; Martin, M. Electrochemical Copper Deposition in Etched Ion Track Membranes. *J. Electrochem. Soc.* **2003**, *150*, C189.

(35) Tian, M.; Wang, J.; Kurtz, J.; Mallouk, T. E.; Chan, M. H. W. Electrochemical Growth of Single-Crystal Metal Nanowires via a Two-Dimensional Nucleation and Growth Mechanism. *Nano Lett.* **2003**, *3*, 919−923.

(36) Bansal, S.; Toimil-Molares, E.; Saxena, A.; Tummala, R. R. Nanoindentation of Single Crystal and Polycrystalline Copper Nanowires. *55th IEEE Electron. Compon. Technol. Conf.* **2005**, *1*, 71−76.

(37) Volklein, F.; Reith, H.; Cornelius, T. W.; Rauber, M.; Neumann, R. The Experimental Investigation of Thermal Conductivity and the Wiedemann-Franz Law for Single Metallic Nanowires. *Nanotechnology* **2009**, *20*, 325706.

(38) Xu, J.; Munari, A.; Dalton, E.; Mathewson, A.; Razeeb, K. M. Silver Nanowire Array-Polymer Composite as Thermal Interface Material. *J. Appl. Phys.* **2009**, *106*, 124310.

(39) Yoon, H.; Deshpande, D. C.; Ramachandran, V.; Varadan, V. K. Aligned Nanowire Growth using Lithography-Assisted Bonding of a Polycarbonate Template for Neural Probe Electrodes. *Nanotechnology* **2008**, *19*, 025304.

(40) Duan, J.; Liu, J.; Mo, D.; Yao, H.; Maaz, K.; Chen, Y.; Sun, Y.; Hou, M.; Qu, X.; Zhang, L. Controlled Crystallinity and Crystallographic Orientation of Cu Nanowires Fabricated in Ion-Track Templates. *Nanotechnology* **2010**, *21*, 365605.

(41) Molares, M. E. T.; Buschmann, V.; Dobrev, D.; Neumann, R.; Scholz, R.; Schuchert, I. U.; Vetter, J. Single-Crystalline Copper Nanowires Produced by Electrochemical Deposition in Polymeric Ion Track Membranes. *Adv. Mater.* **2001**, *13*, 62−65.

(42) Moore, A. L.; Pettes, M. T.; Zhou, F.; Shi, L. Thermal Conductivity Suppression in Bismuth Nanowires. *J. Appl. Phys.* **2009**, *106*, 034310.

(43) Riveros, G.; Green, S.; Cortes, A.; Gómez, H.; Marotti, R. E.; Dalchiele, E. A. Silver Nanowire Arrays Electrochemically Grown into Nanoporous Anodic Alumina Templates. *Nanotechnology* **2006**, *17*, 561−570.

(44) Cahill, D. G. Thermal Conductivity Measurement from 30 to 750 K: the 3w Method. *Rev. Sci. Instrum.* **1990**, *61*, 802−808.

(45) Kim, J. H.; Feldman, A.; Novotny, D. Application of the Three Omega Thermal Conductivity Measurement Method to a Film on a Substrate of Finite Thickness. *J. Appl. Phys.* **1999**, *86*, 3959.

(46) Dames, C.; Chen, G. 1ω, 2ω, and 3ω Methods for Measurements of Thermal Properties. *Rev. Sci. Instrum.* **2005**, *76*, 124902.

(47) Tong, T.; Majumdar, A. Reexamining the 3-omega Technique for Thin Film Thermal Characterization. *Rev. Sci. Instrum.* **2006**, *77*, 104902.

(48) Bauer, M. L.; Norris, P. M. General Bidirectional Thermal Characterization via the 3omega Technique. *Rev. Sci. Instrum.* **2014**, *85*, 064903.

(49) Roy-Panzer, S.; Kodama, T.; Lingamneni, S.; Panzer, M. A.; Asheghi, M.; Goodson, K. E. Thermal Characterization and Analysis of Microliter Liquid Volumes using the Three-Omega Method. *Rev. Sci. Instrum.* **2015**, *86*, 024901.

(50) Barako, M. T.; Weisse, J. M.; Roy, S.; Kodama, T.; Dusseault, T. J.; Motoyama, M.; Asheghi, M.; Prinz, F. B.; Zheng, X.; Goodson, K. E. Thermal Conduction in Nanoporous Copper Inverse Opal Films. In *14th IEEE Intersociety Conference on Thermal Thermomechanical Phenomena Electronic Systems*; IEEE: Piscataway, NJ, USA, 2014; pp 736−74310.1109/ITHERM.2014.6892354.

(51) Carslaw, H.; Jaeger, J. *Heat in Solids*; Clarendon Press: Oxford, UK, 1959.

(52) Feldman, A. Algorithm for Solutions of the Thermal Diffusion Equation in a Stratified Medium with a Modulated Heating Source. *High Temp.−High Pressures* **1999**, *31*, 293−298.

(53) Touloukian, Y.; Powell, R.; Ho, C.; Klemens, P. Thermophysical Properties of Matter − The TPRC Data Series. Volume 1. *Thermal Conductivity − Metallic Elements and Alloys*; DTIC Document; DTIC: Ft. Belvoir, WA, USA, 1970.

(54) Mayadas, A.; Shatzkes, M. Electrical-Resistivity Model for Polycrystalline Films: the Case of Arbitrary Reflection at External Surfaces. *Phys. Rev. B* **1970**, *1*, 1382−1389.

(55) Nan, C.-W.; Birringer, R.; Clarke, D. R.; Gleiter, H. Effective Thermal Conductivity of Particulate Composites with Interfacial Thermal Resistance. *J. Appl. Phys.* **1997**, *81*, 6692.

(56) Nan, C. W.; Shi, Z.; Lin, Y. A Simple Model for Thermal Conductivity of Carbon Nanotube-Based Composites. *Chem. Phys. Lett.* **2003**, *375*, 666−669.

(57) Kim, T. H.; Zhang, X. G.; Nicholson, D. M.; Evans, B. M.; Kulkarni, N. S.; Radhakrishnan, B.; Kenik, E. A.; Li, A. P. Large Discrete Resistance Jump at Grain Boundary in Copper Nanowire. *Nano Lett.* **2010**, *10*, 3096−3100.